Front. Optoelectron. 2016, 9(3): 353–361
DOI 10.1007/s12200-016-0598-z

RESEARCH ARTICLE

Performance improvement by enhancing the well-barrier hole burning in a quantum well semiconductor optical amplifier

Tong CAO, Xinliang ZHANG (✉)

Wuhan National Laboratory for Optoelectronics, School of Optical and Electronic Information,
Huazhong University of Science and Technology, Wuhan 430074, China

© Higher Education Press and Springer-Verlag Berlin Heidelberg 2016

Abstract In this paper, we demonstrated a novel physical mechanism based on the well-barrier hole burning enhancement in a quantum well (QW) semiconductor optical amplifier (SOA) to improve the operation performance. To completely characterize the physical mechanism, a complicated theoretical model by combining QW band structure calculation with SOA's dynamic model was constructed, in which the carrier transport, interband effects and intraband effects were all taken into account. The simulated results showed optimizing the thickness of the separate confinement heterostructure (SCH) layer can effectively enhance the well-barrier hole burning, further enhance the nonlinear effects in SOA and reduce the carrier recovery time. At the optimal thickness, the SCH layer can store enough carrier numbers, and simultaneously the stored carriers can also be fast and effectively injected into the QWs.

Keywords nonlinear optics, optical signal processing, semiconductor optical amplifier (SOA)

1 Introduction

Semiconductor optical amplifiers (SOAs) show significant promise in all-optical signal processing, such as wavelength conversion [1–3], logic function [4–6], format conversion [7–9] and signal regeneration [10–12], owing to various nonlinearities, small-footprint, cost-effectiveness, low-driving requirements and ability for on-chip processing. However, the SOAs performance for high-data-rate (greater than 10 Gb/s) operation is limited by the intrinsic carrier lifetime, which is on the order of a few hundred picoseconds in typical SOAs. To overcome this problem, many schemes have been proposed, such as exploiting an additional optical injection in the gain region [13] or toward transparency wavelength [14–16], employing detuning optical filter [17,18], using P-type-doped multiple quantum wells (MQWs) [19], optimizing QW structure to enhance differential gain [20] and designing a step QW [21] or asymmetric QW structure [22] or using the quantum dot (QD) structure [23]. For the schemes using the additional light [13–16], when the injected wavelength is selected in the gain region, the available gain of the SOA will be significantly compressed; while the injected wavelength operating near the transparency wavelength, the available gain will remain but have to pay the cost of rather high optical injection power level. For the schemes using the detuning optical filter [17,18], the slow recovery process in SOA has not been changed and the acceleration of the carrier recovery time is realized by the detuning optical filter to eliminate the slow recovery process in the SOA. However, the slow recovery process determined by the interband effects are the strongest process in SOA, if this process is largely suppressed, the output power level of the converted signal is rather low. Therefore, in our opinion, optimizing the material [19] or gain region structures [20–23] are the fundamental methods to accelerate the carrier recovery time. It is interesting to find a novel scheme in compatible with the optimized gain region schemes [19–22].

In this paper, we found that just optimizing the thickness of the separate confinement heterostructure (SCH) layer can effectively reduce the carrier recovery time. The former QW optimized structures can continue to be used in the gain region. Our scheme was based on the well-barrier hole burning enhancement. The well-barrier hole burning was proposed by Rideout et al. [24], which was used to explain the anomalously high damping behavior of QW lasers. The well-barrier hole burning describes the equilibrium carrier thermal distribution between the wells and the confinement region induced by photon density

Received January 7, 2016; accepted June 15, 2016

E-mail: xlzhang@mail.hust.edu.cn

change. It is strongly related to the transport time from the doped cladding regions to wells, which is the sum of the ambipolar diffusion time across the SCH region and the capture time into wells. The capture time into the QWs is on the order of 0.5–1 ps, which is difficult to change [25]. However, if the SCH thickness is modified, the ambipolar diffusion time is easy to modify. That is to say, optimizing the SCH thickness can enhance the well-barrier hole burning and reduce the carrier recovery time. To the best of our knowledge, there is no report on optimizing SCH thickness to reduce the recovery time. On the other hand, this work is necessary. In Ref. [19], the SCH thickness was selected as 10 nm, and in Ref. [26]. it was 5 nm; while in Ref. [27], the SCH thickness was selected as 100 nm. There is no judgment rule on how to select the SCH thickness. To study the SCH thickness effect on the SOA performance, we constructed a comprehensive model by combining the band structure calculation with SOA dynamic model, in which carrier transport, optical confinement factor calculation, interband effects and intraband effects were all taken into account. The simulated result demonstrated there was an optimal SCH thickness. At the optimal thickness, the SCH layer can store enough carrier numbers and the stored carriers can be fast and effectively injected into the QWs, which guarantee the strongest nonlinear effects with the shortest recovery time.

The rest of this paper is organized as follows. In Section 2, a description of the rate-equation, including carrier transport, carrier density and temperature dynamics, and the corresponding gain model, is given. In Section 3, the calculated results of the carrier recovery acceleration are presented. Finally, conclusions are given in Section 4.

2 QW SOA model

To study the characteristics of the well-barrier hole burning in a QW SOA, a detailed model is required. A description of the rate-equation, including carrier transport, carrier density and temperature dynamics, and the corresponding gain model, is given.

2.1 Carrier dynamics and operation principle

The typical structure of a QW SOA contains two SCH layers, the doped cladding regions and the QWs [28]. The carrier transport processes are illustrated in Fig. 1. First, electrons and holes transport from the doped cladding regions across the SCH determined by the current continuity equations. Then the electrons and holes are captured by the QWs. The transport between the QWs consists of two concurrent processes [26]: thermionic emission followed by transport across the barriers plus captured in the adjacent QW on the other side and tunneling through the barriers. For the simplicity of our simulation, charge neutrality is assumed in both regions. Each transport is characterized by its typical time of the physical mechanism [28], as shown in Fig. 1.

The transport time from the doped cladding regions to the wells is modeled as

$$\tau_s = \tau_{cap} + \tau_{SCH}, \tag{1}$$

where τ_{cap} is the capture time into the QWs and τ_{SCH} is the ambipolar diffusion time across the SCH region. The ambipolar time is proportional to the square of the SCH thickness and inversely to the diffusion coefficient [28]

$$\tau_{SCH} = \frac{t_{SCH}^2}{2D_a} = \frac{1}{2}\left(\frac{t_{SCH}^2}{2D_n} + \frac{t_{SCH}^2}{2D_p}\right), \tag{2}$$

where D_a is an ambipolar diffusion coefficient, t_{SCH}, D_n and D_p are the thickness of the SCH layer, the electron diffusion coefficient and hole diffusion coefficient, respectively.

The transport time between the wells can be characterized as

$$\frac{1}{\tau_{inter_c}} = \frac{1}{\tau_e + \tau_{bar} + \tau_{cap}} + \frac{1}{\tau_{tun}}, \tag{3}$$

where τ_{bar}, τ_{cap}, and τ_{tun} are the diffusion time across the barriers, capture time into the adjacent QW, and tunneling time through the barriers, respectively. τ_e is the thermionic emission lifetime from the QW [28]

$$\tau_e = \left(\frac{2\pi m^* t_{well}^2}{k_B T}\right)^{1/2} \exp\left(\frac{E_B}{k_B T}\right), \tag{4}$$

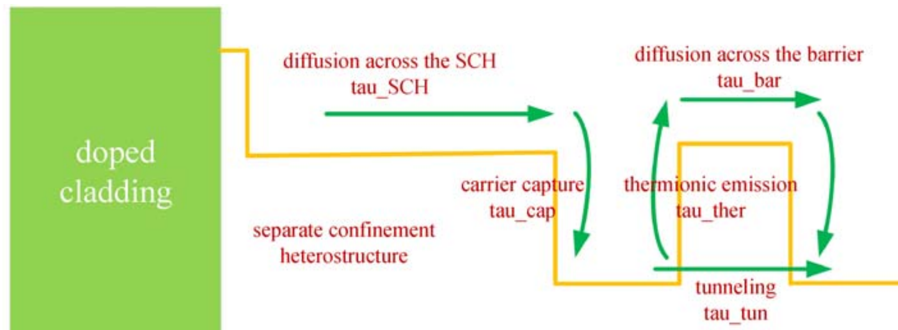

Fig. 1 Schematic diagram of a QW SOA with a SCH layer used in SOA model

where E_B, m^*, k_B, T and t_{well} are the effective barrier height, carrier effective mass, Boltzman constant, temperature in K, and thickness of each well, respectively.

In our material system, the thermionic emission time is on the order of few picoseconds, while the tunneling time is on the order of few femtoseconds (~90 fs) [26]. Thus the carrier transport between the QWs is mainly determined by the tunneling effect. As the tunneling time is rather short, the carrier density distribution in different wells on the order of a few picoseconds can be assumed the same. Hence, one carrier density rate equation can describe all the QWs. On the other hand, an additional carrier rate equation is required to describe the carrier distribution in the SCH layer. The describing method is similar to that in the 2N model [29]. For the SCH layer and QWs, one can write explicitly

$$\frac{\mathrm{d}N_{\mathrm{SCH}}}{\mathrm{d}t} = \frac{\eta_{\mathrm{inj}} I}{qLwt_{\mathrm{SCH}}} - \frac{N_{\mathrm{SCH}}}{\tau_{\mathrm{s}}} - R_{\mathrm{SCH}}(N_{\mathrm{SCH}}) + \frac{N_{\mathrm{w}}}{\tau_{\mathrm{e}}} \frac{t_{\mathrm{well_total}}}{t_{\mathrm{SCH}}}, \tag{5}$$

$$\frac{\mathrm{d}N_{\mathrm{w}}}{\mathrm{d}t} = \frac{N_{\mathrm{SCH}}}{\tau_{\mathrm{s}}} \frac{t_{\mathrm{SCH}}}{t_{\mathrm{well_total}}} - \frac{N_{\mathrm{w}}}{\tau_{\mathrm{e}}} - R_{\mathrm{w}}(N_{\mathrm{w}}) - \sum_{i=\mathrm{pump,probe}} v_{\mathrm{g}} g_i S_i, \tag{6}$$

where η_{inj} is the injection efficiency, L is the active layer length, w is the active layer thickness, v_g is the group velocity, $t_{well_total} = M \times t_{well}$ is the total thickness of the QWs, M is the number of the QWs, S_i is the photon density in the well region of pump or probe signal, whose relationship with the pump or probe power can be described as

$$S_i = \frac{\Gamma}{wt_{\mathrm{well_total}}} \frac{P_i v_{\mathrm{g}}}{\hbar\, \omega_i}, \tag{7}$$

where Γ is the optical confinement factor, which is calculated by [30]

$$\Gamma = \sum_{j=1}^{M} \int_0^w \int_0^{(j-1)^* t_{\mathrm{barrier}} + j t_{\mathrm{well}}} |F(x,y)|^2 \mathrm{d}x\mathrm{d}y \Big/ \int_{-\infty}^{\infty} \int_{-\infty}^{\infty} |F(x,y)|^2 \mathrm{d}x\mathrm{d}y, \tag{8}$$

where $F(x,y)$ is the transverse distribution obtained by the COMSOL Multiphysics Software, $t_{barrier}$ is the barrier thickness. R_{SCH} and R_w are the spontaneous recombination rates in the SCH layers and QWs, which are given by the following equations

$$R_{\mathrm{SCH}}(N_{\mathrm{SCH}}) = A_{\mathrm{SCH}} N_{\mathrm{SCH}} + B_{\mathrm{SCH}} N_{\mathrm{SCH}}^2 + C_{\mathrm{SCH}} N_{\mathrm{SCH}}^3, \tag{9}$$

$$R_{\mathrm{w}}(N_{\mathrm{w}}) = A_{\mathrm{w}} N_{\mathrm{w}} + B_{\mathrm{w}} N_{\mathrm{w}}^2 + C_{\mathrm{w}} N_{\mathrm{w}}^3, \tag{10}$$

where A_{SCH} and A_w, B_{SCH} and B_w, C_{SCH} and C_w are the recombination constants caused by trapping sites, the bimolecular spontaneous radiative recombination coefficients and the Auger recombination coefficients in the SCH and the QWs regions, respectively.

In analogy with spectral hole burning, the photon density changes the distribution of the carrier numbers between the SCH and QW regions, as Eqs. (5) and (6) show [24]. As shown in [24], the nonlinear gain suppression factor due to the well-barrier hole burning is proportional to the transport time from the doped cladding regions to the wells, which is the sum of the ambipolar diffusion time across the SCH region and the capture time into wells, as Eq. (1) shows. The capture time τ_{cap} into the QWs is about 0.5–1 ps, which is difficult to change [25]. However, if SCH thickness is modified, the diffusion time τ_{SCH} is easy to change, according to Eq. (2). This is the key mechanism why optimizing the SCH thickness can enhance the well-barrier hole burning, further enhance the nonlinear effect in SOA and reduce the recovery time.

2.2 Carrier temperature dynamics

The ultrafast carrier temperature dynamics are considered in our model. Similar to the carrier density rate equation in QWs, only one carrier temperature rate equation is required, which can be described by [31]

$$\frac{\mathrm{d}T_{\mathrm{w}}}{\mathrm{d}t} = \frac{1}{\partial U_{\mathrm{w}}/\partial T_{\mathrm{w}}} \left(\frac{\mathrm{d}U_{\mathrm{w}}}{\mathrm{d}t} - \frac{\partial U_{\mathrm{w}}}{\partial N_{\mathrm{w}}} \frac{\mathrm{d}N_{\mathrm{w}}}{\mathrm{d}t} \right) - \frac{T_{\mathrm{w}} - T_0}{\tau_{\mathrm{T}}}, \tag{11}$$

$$\frac{\mathrm{d}U_{\mathrm{w}}}{\mathrm{d}t} = -\sum_i (\hbar\, \omega_i - E_{\mathrm{g}}) v_{\mathrm{g}} g_i S_i + \sum_i \hbar\, \omega_i v_{\mathrm{g}} \alpha_{\mathrm{Fc}} N_{\mathrm{w}} S_i, \tag{12}$$

where T_0 is the lattice temperature, τ_T is the intraband scattering time, U is the energy density, E_g is the material bandgap, α_{Fc} is the absorption coefficient due to free carrier absorption. The details of Eqs. (11) and (12) and corresponding parameters can be found in Ref. [31].

2.3 Traveling equations and optical gain model

The traveling wave rate equations are modeled as

$$\frac{\mathrm{d}S_i}{\mathrm{d}z} = (\Gamma g_i - \alpha_{\mathrm{Fc}} N_{\mathrm{w}} - \alpha_{\mathrm{int}}) S_i, \tag{13}$$

$$\frac{\mathrm{d}\Phi_i}{\mathrm{d}z} = -\Gamma \frac{2\pi}{\lambda} (\Delta n_i + \Delta n_{\mathrm{Fc}i}), \tag{14}$$

where α_{int} is the internal loss, Δn_{Fci} is the refractive index-change due to plasma effect, which is described by [32]

$$\Delta n_{\mathrm{Fc}i}=\frac{e^2\lambda_i^2N_\mathrm{w}}{8\pi^2c^2\varepsilon_0n_\mathrm{r}}\left(\frac{1}{m_\mathrm{e}}+\frac{m_\mathrm{hh}^{1/2}+m_\mathrm{lh}^{1/2}}{m_\mathrm{hh}^{3/2}+m_\mathrm{lh}^{3/2}}\right),\tag{15}$$

where c is the velocity of light in the free space, n_r is the background index, ε_0 is the permittivity in free space, m_e, m_hh, m_lh are the effective masses of the electrons, heavy holes and light holes, respectively.

In the active region of the QW SOA, the optical material gain coefficient and refractive index-change can be written as [33]

$$g_i(\hbar\,\omega)=\frac{q^2\pi}{n_\mathrm{r}c\varepsilon_0{m_0}^2\omega t_\mathrm{well}}\times\sum_{\eta=\uparrow,\downarrow}\sum_{\sigma=U,L}\sum_{n,m}\int|\hat{e}\cdot M_{nm}^{\eta\sigma}(k_\mathrm{t})|^2\times\frac{(\gamma/\pi)}{(E_{\sigma,nm}^{\mathrm{cv}}(k_\mathrm{t})-\hbar\,\omega)^2+\gamma^2}\times(f_n^\mathrm{c}(k_\mathrm{t})+f_{\sigma m}^\mathrm{v}(k_\mathrm{t})-1)\times\frac{k_\mathrm{t}\mathrm{d}k_\mathrm{t}}{2\pi},\tag{16}$$

$$\Delta n_i=\frac{q^2\hbar^2}{\varepsilon_0{m_0}^2n_\mathrm{r}t_\mathrm{well}}\sum_{\eta=\uparrow,\downarrow}\sum_{\sigma=U,L}\sum_{n,m}\int|\hat{e}\cdot M_{nm}^{\eta\sigma}(k_\mathrm{t})|^2\times\frac{(f_n^\mathrm{c}(k_\mathrm{t})+f_{\sigma m}^\mathrm{v}(k_\mathrm{t})-1)}{(E_{\sigma,nm}^{\mathrm{cv}}(k_\mathrm{t})-\hbar\,\omega)^2+\gamma^2}\times\frac{E_{\sigma,nm}^{\mathrm{cv}}(k_\mathrm{t})-\hbar\,\omega}{E_{\sigma,nm}^{\mathrm{cv}}(k_\mathrm{t})(E_{\sigma,nm}^{\mathrm{cv}}(k_\mathrm{t})+\hbar\,\omega)}\times\frac{k_\mathrm{t}\mathrm{d}k_\mathrm{t}}{2\pi},\tag{17}$$

where q is the magnitude of the electron charge, m_0 is the electron rest mass in free space, $\hat{e}$ is the polarization vector of the optical electric field, γ is the half linewidth of the Lorentzian function, k_t is the real transverse wave number and, $E_{\sigma,nm}^{\mathrm{cv}}(k_\mathrm{t})=E_n^\mathrm{c}(k_\mathrm{t})-E_{\sigma,m}^\mathrm{v}(k_\mathrm{t})$ where $E_n^\mathrm{c}(k_\mathrm{t})$ and $E_{\sigma,m}^\mathrm{v}(k_\mathrm{t})$ are eigenenergies in the conduction and the valence band. $M_{nm}^{\eta\sigma}(k_\mathrm{t})$ is the momentum matrix element, which is defined as

$$M_{nm}^{\eta\sigma}(k_\mathrm{t})=\langle\psi_{m,k_\mathrm{t}}^{\mathrm{v}\sigma}|p|\psi_{m,k_\mathrm{t}}^{\mathrm{c}\eta}\rangle,\tag{18}$$

where p is the momentum operator. For transverse electric (TE) mode and transverse magnetic (TM) mode, the momentum matrix element are separately expressed as

$$|M_\mathrm{TE}|^2=|\hat{x}\cdot M_{nm}^{\eta\sigma}(k_\mathrm{t})|^2=|\hat{y}\cdot M_{nm}^{\eta\sigma}(k_\mathrm{t})|^2=\frac{{M_\mathrm{b}}^2}{4}\{|\langle g_{m,\mathrm{lh}}^\sigma+\sqrt{2}g_{m,\mathrm{so}}^\sigma|\phi_n\rangle|^2+3|\langle g_{m,\mathrm{hh}}^\sigma|\phi_n\rangle|^2\},\tag{19}$$

$$|M_\mathrm{TM}|^2=|\hat{z}\cdot M_{nm}^{\eta\sigma}(k_\mathrm{t})|^2={M_\mathrm{b}}^2|\langle g_{m,\mathrm{lh}}^\sigma-\frac{1}{\sqrt{2}}g_{m,\mathrm{so}}^\sigma|\phi_n\rangle|^2,\tag{20}$$

where ${M_\mathrm{b}}^2$ is the bulk value of the momentum matrix element, $\phi_n(z)$ is the envelope function of the nth conduction subband, $g_{m,\mathrm{hh}}^\sigma(z;k_\mathrm{t})$, $g_{m,\mathrm{lh}}^\sigma(z;k_\mathrm{t})$, $g_{m,\mathrm{so}}^\sigma(z;k_\mathrm{t})$ are the hole envelope functions of the mth valence subband. As Eqs. (19) and (20) show, the TE mode momentum matrix element is mainly determined by overlap integral value of the envelop functions between conduction electrons and the heavy holes, while the TM mode momentum matrix is determined by that between conduction electrons and the light holes. $f_n^\mathrm{c}(k_\mathrm{t})$ and $f_{\sigma m}^\mathrm{v}(k_\mathrm{t})$ are the Fermi functions of electrons and holes, which are described as

$$f_n^\mathrm{c}(k_\mathrm{t})=\frac{1}{1+\exp\left(\frac{E_\mathrm{nc}(k_t)-E_\mathrm{fc}(N_\mathrm{w},T_\mathrm{w})}{KT_\mathrm{w}}\right)},\tag{21}$$

$$f_{\sigma m}^\mathrm{v}(k_\mathrm{t})=\frac{1}{1+\exp\left(\frac{E_\mathrm{mv}(N_\mathrm{w},T_\mathrm{w})-E_\mathrm{mv}(k_\mathrm{t})}{KT_\mathrm{w}}\right)},\tag{22}$$

where E_fc and E_mv are the quasi-Fermi levels for electrons and holes, respectively. Equations (21) and (22) show the Fermi functions will change as long as the carrier density N_w and carrier temperature T_w change, thus the material gain and refractive-index will change. The band structure is obtained by the $k\cdot p$ method [33].

The main simulation parameters are listed in Table 1.

Table 1 Main modeling parameters

quantity		value
L	SOA length	500×10^{-6} m
w	SOA width	2.0×10^{-6} m
A_w	nonradiative recombination constant	3.5×10^{8} s^{-1}
B_w	bimolecular recombination constant	5.6×10^{-16} m$^3\cdot$s^{-1}
C_w	Auger recombination constant	3.0×10^{-41} m$^6\cdot$s^{-1}
A_SCH	nonradiative recombination constant	5.0×10^{8} s^{-1}
B_SCH	bimolecular recombination constant	8.0×10^{-16} m$^3\cdot$s^{-1}
C_SCH	Auger recombination constant	5.0×10^{-41} m$^6\cdot$s^{-1}
η_inj	injection efficiency	0.8
α_int	internal loss	2×10^{3} m^{-1}
D_n	electron diffusion coefficient	1.19×10^{-2} m$^4\cdot$s^{-1}
D_p	hole diffusion coefficient	3.885×10^{-4} m$^4\cdot$s^{-1}
τ_cap	capture time	1.0 ps
M	number of QWs	8
$t_\mathrm{well_total}$	total QW thickness	$8\times8=64$ nm
t_SCH	SCH thickness	variable
α_Fc	free carrier absorption	2.0×10^{-21} m^2
τ_T	intraband scatting time	1.5 ps

3 Calculated results and discussion

In this Section, first the QW SOA is designed to operate at C band. Before the dynamics model calculation, the SCH thickness effect on the optical confinement factor should be considered, because when the SCH thickness changes, the optical field distribution in the QW will be slightly change, thus resulting in the optical confinement factor variation. The optical confinement factor has an obvious effect on the carrier recovery time [14]. To comprehensively characterize the SCH thickness effect on the SOA performance, the calculation of optical confinement factor versus the SCH thickness is necessary. Finally, the SCH thickness effect on the SOA performance is given. The optimal SCH thickness has been found and at the optimal thickness, the SOA has the strongest nonlinear effect with the shortest recovery time.

3.1 Design of active region

The material system is selected as InGaAs/InGaAsP. The material of the QWs is $In_{1-x}Ga_xAs$, which is surrounded by 8 nm $In_{0.7322}Ga_{0.2678}As_{0.5810}P_{0.4190}$ barrier. The barrier's lattice is matched to the InP substrate and bandgap wavelength is 1.3 μm. When the gallium mole fraction (x) equals 0.47, the well is lattice-matched to the InP substrate. When x is larger than 0.47, tensile strain is introduced and when x is smaller than 0.47, compressive strain is introduced. To easier fabricate the device, we choose the gallium mole fraction equals 0.47 with no strain. In this paper, the device is designed to operate at C band. To meet this demand, the band structure versus the thickness of the QWs is investigated and eventually the QW thickness is selected as 8 nm. At 8 nm QW thickness, the band structures obtained using the Eqs. (23) and (24) are shown in Figs. 2(a) and 2(b). The bandgap wavelength is 1567.4 nm. There is only one subband in the conduction band and there are four subbands in the valence band. The hole envelope functions shows all the valence subbands except the second subband are the heavy hole bands (HH1, HH2, HH3) and the second is the light hole band (LH1). As discussed in Section 2, the TE mode gain is mainly determined by the heavy holes and TM mode gain is determined by the light holes. Thus we can predict TE gain is much larger than the TM gain. The optical material gain versus the wavelength verifies this point as Fig. 2(c) shows. As the gain of the device is mainly determined by the gain of TE mode, only TE mode gain is taken into account in this paper.

3.2 SCH effect on optical confinement factor

The geometric structure of the active region is shown in Fig. 3. The material of the SCH layer is the same as that of the barrier and there are eight QWs. When the SCH thickness varies, the transverse field distribution will also change, which leads to the variation of the optical confinement factor. Therefore the SCH thickness effect on the optical confinement factor should be first studied and taken into account in our SOA model. The simulated result is shown in Fig. 4. The transverse field distribution at 45 nm SCH thickness is given in Fig. 4(a). Although the QW refractive index is rather high (3.6088), the total thickness of the QWs (64 nm) is too thin in contrast to that of the whole structure, so the confinement factor is limited to 0.124. The transverse field distributions of other SCH thicknesses are similar to the distribution in Fig. 4(a). Figure 4(b) shows that the optical confinement factor increases with the SCH thickness increasing until the SCH thickness reaches 120 nm then slightly decreases. When the SCH thickness is too thin, the optical field is mainly distributed in the substrate and InP. Then with the SCH thickness increasing, more optical field comes to focus in the active region due to the refractive index of SCH thickness larger than that of InP substrate. This is the reason why the optical confinement factor increases. However, when the SCH thickness is too thick, the optical field will be more spread in the SCH layer due to its refractive index smaller than the QW, which results in the optical confinement factor slightly decreasing.

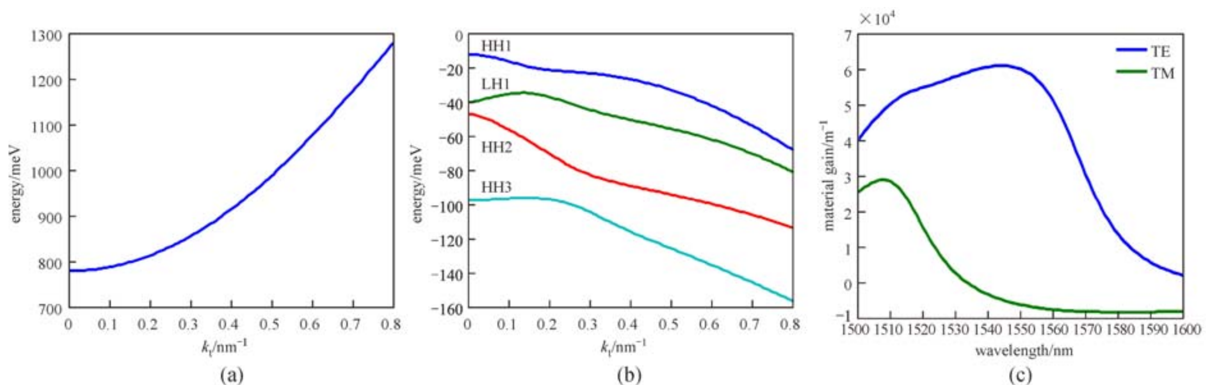

Fig. 2 (a) Conduction band structure; (b) valence band structure. The gallium mole fraction is 0.47 and the well thickness is selected as 8 nm; (c) material gains of TE and TM mode versus the wavelength, the carrier density is 2.2×10^{24} m^{-3}

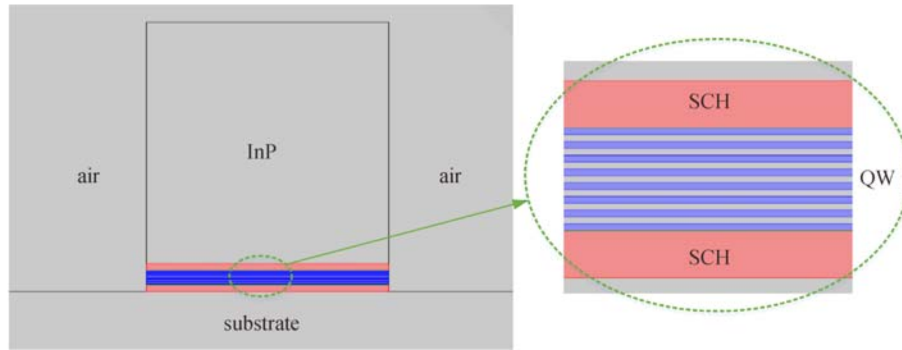

Fig. 3 Geometric structure of the active region

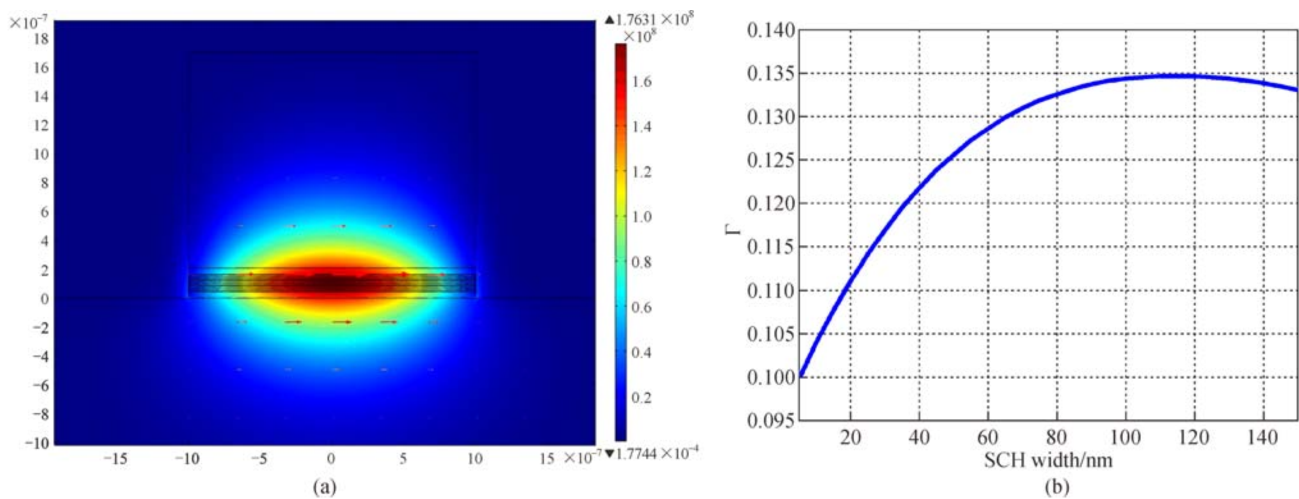

Fig. 4 (a) Transverse field distribution at 45 nm SCH thickness; (b) optical confinement factor versus the SCH thickness

3.3 SCH effect on SOA performance

Generally, the carrier recovery time in the SOA is studied using the pump-probe technique. The setup is shown in Fig. 5. The pump signal is used to modulate the carrier density and carrier temperature in the SOA, and the probe signal is to measure the carrier recovery time. The bandpass filter (BPF) is used to filter the probe signal after the SOA. The carrier recovery time is obtained by measuring the time of the normalized probe signal from 10% to 90%.

In our simulation, the wavelengths of pump and probe signals are 1555 and 1545 nm, respectively. The probe signal is a continuous wave (CW) beam and assumed to be 0 dBm. The pump signal is assumed to be an ideal Gaussian pulse with 2.8 ps full width at half maximum (FWHM) and −3.51 dBm average power. Combining the calculated results of the optical confinement factor with SOA dynamic model, the SCH thickness effect on the carrier recovery time is investigated in Fig. 6. First, we discuss the situation of 150 mA biased current. When the SCH thickness equals 45 nm, the recovery time reaches its minimal value. We select three samples to compare the amplitude and phase recovery process of the converted

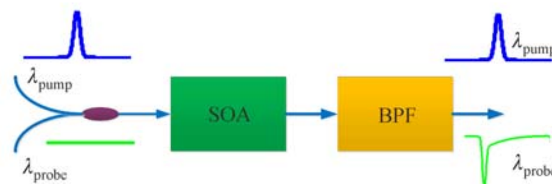

Fig. 5 Pump-probe technique to measure the carrier recovery time

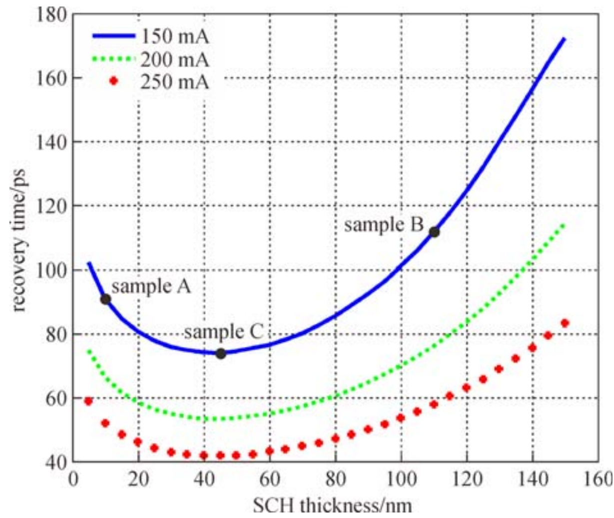

Fig. 6 Carrier recovery time versus the SCH thickness

probe signal. The SCH thicknesses of sample A and B are 10 and 110 nm, respectively. Sample C is the optimal SCH thickness calculated using our model. For sample B, in Ref. [27] it is selected as 100 nm, while here we choose 110 nm. The reason is that the SCH bandgap wavelength in Ref. [27] is 1.2 μm, while in our material system is 1.3 μm. To offer the same confined effects for the carriers, the SCH thickness is enlarged to 110 nm. The amplitude and phase dynamics of the probe signal for the three samples are shown in Fig. 7. It is obvious that sample C has the shortest recovery time. When the SCH thickness is too thin, the carrier in the SCH layer can easily and fast move into the QWs. However, the carrier numbers stored in the SCH layer are not so many due to the thin thickness, which leads to the well-barrier hole burning is not strong enough. As shown in Fig. 7(a), the carrier in sample A can easily and fast recover from 40 to 50 ps. However, the SCH layer is too thin, there is not enough carrier stored in the layer. From 50 ps afterwards, carrier recovery process slows down. On the other hand, when the SCH thickness is too thick, the SCH layer can store a lot of carriers; however, the carrier diffusion time is too long and the carrier cannot effectively move into the QWs. The well-barrier hole burning is also limited. This is the reason why there is a fast recovery process enhancement from 40 to 42 ps for sample B in Figs. 7(a) and 7(b). At this time, the carrier is significantly depleted by the pump signal and the replenishment into the QWs is largely limited, resulting in that the carrier temperature is significantly heated. From 42 ps afterwards, the sample B has a rather slow recovery process. So there must be an optimal SCH thickness to ensure the SCH layer can store enough carrier numbers and simultaneously the stored carriers can also be fast and effectively injected into the QWs. At this optimal thickness, the well-barrier hole burning is the strongest, which guarantees the shortest recovery time. This point can be partly verified in Fig. 7(b). The sample C has the shortest recovery time and it also has the strongest phase change. As is well known, the phase change determines the strength of the cross-phase modulation (XPM). That is to say, the sample C has the strongest XPM effect. Actually, the amplitude dip depth of not normalized amplitude of the converted probe signal for sample C is also the largest, which partly verifies that the cross-gain modulation (XGM) in sample C is the strongest. Using the sample C, the carrier recovery time can be reduced and at the same time the nonlinear effects can also be enhanced.

The tendency of the SCH thickness effect on the carrier recovery at other current is similar to that of 150 mA as shown in Fig. 6. Increasing the current, the carrier density in the QWs is improved, thus the effective carrier lifetime is reduced as shown in Eq. (10). Then the carrier recovery

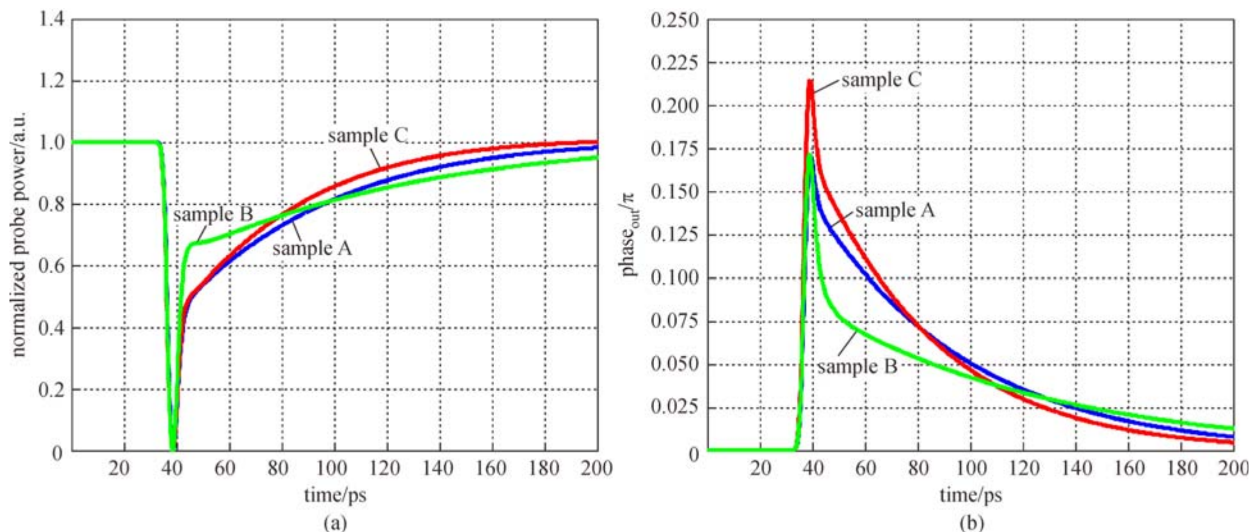

Fig. 7 (a) Amplitude dynamics of probe signal for different samples; (b) phase dynamics of probe signal for different samples

time is reduced [14]. On all situations, the sample C has the shortest recovery time. In a word, by enhancing the well-barrier hole burning, we can reduce the recovery time and simultaneously enhance the nonlinear effects.

4 Conclusions

In conclusion, a complicated theoretical model by combining QW band structure calculation with the SOA dynamic model has been developed, in which carrier transport, carrier density and carrier temperature variation are all taken into account. Based on the SOA model, the well-barrier hole burning is enhanced by optimizing the SCH thickness. At the optimized SCH thickness, the carrier recovery time has been significantly reduced and nonlinear effects has also been enhanced in contrast to the typical MQW SOAs (samples A and B). Through the proper design of the SCH thickness, the QW SOA may show better performance in high-speed optical signal processing.

Acknowledgements This work was supported by the National Basic Research Program of China (No. 2011CB301704), the National Natural Science Found for Distinguished Yong Scholars (No. 61125501), the National Natural Science Foundation of China (NSFC) Major International Joint Research Project (Grant No. 61320106016) and Scientific and Technological Innovation Cross Team of Chinese Academy of Sciences.

References

1. Durhuus T, Mikkelsen B, Joergensen C, Lykke Danielsen S, Stubkjaer K E. All-optical wavelength conversion by semiconductor optical amplifiers. Journal of Lightwave Technology, 1996, 14(6): 942–954
2. Liu Y, Tangdiongga E, Li Z, de Waardt H, Koonen A M J, Khoe G D, Shu X, Bennion I, Dorren H J S. Error-free 320-Gb/s all-optical wavelength conversion using a single semiconductor optical amplifier. Journal of Lightwave Technology, 2007, 25(1): 103–108
3. Krzczanowicz L, Connelly M J. 40 Gb/s NRZ-DQPSK data all-optical wavelength conversion using four wave mixing in a bulk SOA. IEEE Photonics Technology Letters, 2013, 25(24): 2439–2441
4. Stubkjaer K E. Semiconductor optical amplifier-based all-optical gates for high-speed optical processing. IEEE Journal of Selected Topics in Quantum Electronics, 2000, 6(6): 1428–1435
5. Dong J, Zhang X, Fu S, Xu J, Shum P, Huang D. Ultrafast all-optical signal processing based on single semiconductor optical amplifier and optical filtering. IEEE Journal of Selected Topics in Quantum Electronics, 2008, 14(3): 770–778
6. Xu J, Zhang X, Zhang Y, Dong J, Liu D, Huang D. Reconfigurable all-optical logic gates for multi-input differential phase-shift keying signals: design and experiments. Journal of Lightwave Technology, 2009, 27(23): 5268–5275
7. Lee C G, Kim Y J, Park C S, Lee H J, Park C. Experimental demonstration of 10-Gb/s data format conversions between NRZ and RZ using SOA-loop-mirror. Journal of Lightwave Technology, 2005, 23(2): 834–841
8. Dong J, Zhang X, Xu J, Huang D, Fu S, Shum P. 40 Gb/s all-optical NRZ to RZ format conversion using single SOA assisted by optical bandpass filter. Optics Express, 2007, 15(6): 2907–2914
9. Banchi L, Presi M, D'Errico A, Contestabile G, Ciaramella E. All-optical 10 and 40 Gbit/s RZ-to-NRZ format and wavelength conversion using semiconductor optical amplifiers. Journal of Lightwave Technology, 2010, 28(1): 32–38
10. Yu Y, Wu W, Huang X, Zou B, Hu S, Zhang X. Multichannel all-optical RZ-PSK amplitude regeneration based on the XPM effect in a single SOA. Journal of Lightwave Technology, 2012, 30(23): 3633–3639
11. Porzi C, Serafino G, Bogoni A, Contestabile G. Phase-preserving amplitude noise compression of 40 Gb/s DPSK signals in a single SOA. Journal of Lightwave Technology, 2014, 32(10): 1966–1972
12. Cao T, Chen L, Yu Y, Zhang X. Experimental demonstration and devices optimization of NRZ-DPSK amplitude regeneration scheme based on SOAs. Optics Express, 2014, 22(26): 32138–32149
13. Yu J, Jeppesen P. Improvement of cascaded semiconductor optical amplifier gates by using holding light injection. Journal of Lightwave Technology, 2001, 19(5): 614–623
14. Pleumeekers J L, Kauer M, Dreyer K, Burrus C, Dentai A G, Shunk S, Leuthold J, Joyner C H. Acceleration of gain recovery in semiconductor optical amplifiers by optical injection near transparency wavelength. IEEE Photonics Technology Letters, 2002, 14(1): 12–14
15. Dupertuis M A, Pleumeekers J L, Hessler T P, Selbmann P E, Deveaud B, Dagens B, Emery J Y. Extremely fast high-gain and low-current SOA by optical speed-up at transparency. IEEE Photonics Technology Letters, 2000, 12(11): 1453–1455
16. Kumar Y, Shenoy M R. A novel scheme of optical injection for fast gain recovery in semiconductor optical amplifier. IEEE Photonics Technology Letters, 2014, 26(9): 933–936
17. Nielsen M L, Mørk J. Increasing the modulation bandwidth of semiconductor-optical-amplifier-based switches by using optical filtering. Journal of the Optical Society of America B, Optical Physics, 2004, 21(9): 1606–1619
18. Liu Y, Tangdiongga E, Li Z, Zhang S, Waardt H D, Khoe G D, Dorren H J S. Error-free all-optical wavelength conversion at 160 Gb/s using a semiconductor optical amplifier and an optical bandpass filter. Journal of Lightwave Technology, 2006, 24(1): 230–236
19. Zhang L, Kang I, Bhardwaj A, Sauer N, Cabot S, Jaques J, Neilson D T. Reduced recovery time semiconductor optical amplifier using p-type-doped multiple quantum wells. IEEE Photonics Technology Letters, 2006, 18(22): 2323–2325
20. Qin C, Huang X, Zhang X. Gain recovery acceleration by enhancing differential gain in quantum well semiconductor optical amplifiers. IEEE Journal of Quantum Electronics, 2011, 47(11): 1443–1450
21. Qin C, Huang X, Zhang X. Theoretical investigation on gain recovery dynamics in step quantum well semiconductor optical amplifiers. Journal of the Optical Society of America B, Optical Physics, 2012, 29(4): 607–613
22. Huang X, Qin C, Yu Y, Zhang X. Acceleration of carrier recovery in

a quantum well semiconductor optical amplifier due to the tunneling effect. Journal of the Optical Society of America B, Optical Physics, 2012, 29(10): 2990–2994

23. Matsuura M, Raz O, Gomez-Agis F, Calabretta N, Dorren H J S. Ultrahigh-speed and widely tunable wavelength conversion based on cross-gain modulation in a quantum-dot semiconductor optical amplifier. Optics Express, 2011, 19(26): B551–B559
24. Rideout W, Sharfin W F, Koteles E S, Vassell M O, Elman B. Well-barrier hole burning in quantum well lasers. IEEE Photonics Technology Letters, 1991, 3(9): 784–786
25. Kersting R, Schwedler R, Wolter K, Leo K, Kurz H. Dynamics of carrier transport and carrier capture in $In_{1-x}Ga_xAs/InP$ heterostructures. Physical Review B: Condensed Matter and Materials Physics, 1992, 46(3): 1639–1648
26. Lysak V V, Kawaguchi H, Sukhoivanov I A, Katayama T, Shulika A V. Ultrafast gain dynamics in asymmetrical multiple quantum-well semiconductor optical amplifiers. IEEE Journal of Quantum Electronics, 2005, 41(6): 797–807
27. Xia F, Wei J, Menon V, Forrest S R. Monolithic integration of a semiconductor optical amplifier and a high bandwidth p-i-n photodiode using asymmetric twin-waveguide technology. IEEE Photonics Technology Letters, 2003, 15(3): 452–454
28. Nagarajan R, Ishikawa M, Fukushima T, Geels R S, Bowers J E. High speed quantum-well lasers and carrier transport effects. IEEE Journal of Quantum Electronics, 1992, 28(10): 1990–2008
29. Tsai C Y, Tsai C Y, Lo Y, Spencer R M, Eastman L F. Nonlinear gain coefficients in semiconductor quantum-well lasers: effects of carrier diffusion, capture, and escape. IEEE Journal of Selected Topics in Quantum Electronics, 1995, 1(2): 316–330
30. Agrawal G P, Olsson N A. Self-phase modulation and spectral broadening of optical pulses in semiconductor laser amplifiers. IEEE Journal of Quantum Electronics, 18989, 25(11): 2297–2306
31. Dailey J M, Koch T L. Simple rules for optimizing asymmetries in SOA-based Mach-Zehnder wavelength converters. Journal of Lightwave Technology, 2009, 27(11): 1480–1488
32. Bennett B R, Soref R A, Alamo J A. Carrier-induced change in refractive index of InP, GaAs and InGaAsP. IEEE Journal of Quantum Electronics, 1990, 26(1): 113–122
33. Chang C, Chuang S. Modeling of strained quantum-well lasers with spin-orbit coupling. IEEE Journal of Selected Topics in Quantum Electronics, 1995, 1(2): 218–229

Tong Cao is currently working toward the Ph.D. degree at the Wuhan National Laboratory for Optoelectronics and School of Optical and Electronic Information, Huazhong University of Science and Technology, Wuhan, China.

His current research interests include all optical signal processing based on semiconductor optical amplifier.

Prof. Xinliang Zhang received the B.S. and Ph.D. degrees from Huazhong University of Science and Technology (HUST), China, in 1992 and 2001. He became a full professor of HUST in 2004. Currently, he is the dean of the school of optical and electronic information, and the deputy director of the Wuhan National Laboratory for Optoelectronics. His research areas cover semiconductor optoelectronic devices for optical interconnection and optical signal processing. He has over 300 publications in prestigious international journals and conferences, including over 160 IEEE Letters/Journals, *Optics Letters* or *Optics Express* papers and 30 OFC/ECOC papers. He holds 10 Chinese patents and 1 US patent. He is a senior member of IEEE and also a member of OSA.